DOI https: //doi. org/10.1007/s11595-024-2946-y

# Preparation and Thermal Stability of AlMoON Based Solar Selective Absorption Coating

**MIN Jie[1,2,3*], YUAN Wenxu[1,2,3], CHEN Yufei[1,2,3], LAN Yapeng[1,2,3], YAN Mengdi[1,2,3], LIU Hanze[4], CHENG Xudong[5], DAI Lu[6*]**

*(1. Hubei Provincial Key Laboratory of Green Materials for Light Industry, Hubei University of Technology, Wuhan 430068, China; 2. Collaborative Innovation Center of Green Light-weight Materials and Processing, Hubei University of Technology, Wuhan 430068, China; 3. School of Materials and Chemical Engineering, Hubei University of Technology, Wuhan 430068, China; 4. School of Industrial Design, Hubei University of Technology, Wuhan 430068, China; 5. State Key Laboratory of Advanced Technology for Materials Synthesis and Processing, Wuhan University of Technology, Wuhan 430070, China; 6. Science and Technology on Thermal Energy and Power Laboratory, Wuhan Second Ship Design & Research Institute, Wuhan 430205, China)*

**Abstract:** AlMoON based solar selective absorption coatings were deposited on stainless steel substrate by magnetron sputtering. The coatings included infrared reflection layer Mo, absorption layer AlMoN, absorption layer AlMoON and antireflection layer AlMoO from bottom to top. The surface of the deposited coatings is flat without obvious defects. The absorptivity and emissivity are 0.896 and 0.09, respectively, and the quality factor is 9.96. After heat treatment at 500 ℃-36 h, the surface roughness of the coating increases, a small number of cracks and other defects appear, and the broken part is still attached to the coating surface. A certain degree of element diffusion occurs in the coatings, resulting in the decline of the optical properties of the coatings. The absorptivity and emissivity are 0.883 and 0.131, respectively, the quality factor is 7.06, and the PC value is 0.0335. The coatings do not fail under this condition and have certain thermal stability.

**Key words:** AlMoON; coating; preparation; thermal stability

## 1 Introduction

As the core component of concentrating solar power (CSP), solar selective absorption coatings can convert solar energy into heat energy, so as to realize light thermal power generation[1-3]. The solar selective absorption coatings have characteristics that are high absorptivity ($\alpha$) in solar radiation range (0.3-2.5 μm) and low emissivity ($\varepsilon$) in infrared range (2.5-25 μm)[4]. At present, thin film coatings are mainly prepared by physical vapor deposition, such as magnetron sputtering and multi arc ion plating[5,6]. Ceramic coatings prepared by physical vapor deposition are widely used in the field of photothermal conversion, and show excellent thermal stability in medium and high temperature environment[7], such as Mo[8-11], Al[12-18], Cr[19-23], Ti[24-26], and prepared coatings show excellent optical properties. For example, the absorptivity and emissivity of Mo-$SiO_2$[9] coatings at 400 ℃ are 0.95 and 0.15, respectively. And the absorptivity and emissivity of the as-deposited AlCrON-based coatings[23] are 0.90 and 0.2, respectively. The performance of the coatings declined after heat treatment at 500 ℃-1 000 h[23], and the absorptivity and emissivity are 0.92 and 0.14, respectively.

In order to effectively improve the selective absorption performance of the coatings to solar energy, the solar selective absorption coatings are gradually developing towards to the direction of multi-layer structure. Guided by the double interference absorption theory[27-29], the solar selective absorption coatings mainly include antireflection layer, absorption layer and infrared reflection layer from the surface to the substrate. According to the previous research, transition metals and their nitride or oxynitride nanoparticles will have a diffusion effect at high temperature, which leads to a certain decline in the optical properties of the coatings, and the columnar structure inside the coatings is conducive to the diffusion behavior of elements[30]. Miao Du,



(Received: Sept. 21, 2023; Accepted: Feb. 18, 2024)

MIN Jie(闵捷): Assoc. Prof.; Ph D; E-mail: whutminj@163.com

*Corresponding authors: MIN Jie(闵捷): Assoc. Prof.; Ph D; E-mail: whutminj@163.com; DAI Lu(代路): Senior Engineer; Ph D; E-mail: sys2017@126.com

Funded by the National Natural Science Foundation of China (No.52002159), the Open Foundation of Hubei Provincial Key Laboratory of Green Materials for Light Industry(No.201611B12), and the Open Fund of Science and Technology on Thermal Energy and Power Laboratory (No.TPL2018A03)

*et al*[31] had prepared a TiAlON-based solar selective absorption coatings, and found that $O_2$ would diffuse with the AlTiN layer, resulting in the formation of an AlTiON films, and the optical properties of the coatings have decreased accordingly. Jyothi *et al*[32] had prepared the TiAlC/TiAlCN/TiAlSiCN/TiAlSiCO/TiAlSiO tandem absorber, and coatings remain thermally stable properties for up to 400 hours at 325 ℃. According to the multilayer structure of the above-mentioned coatings, Wang[33] had proposed a approach to deal with the above problems, using the method of multi-arc ion plating to prepare the Cr/AlCrN/AlCrON/AlCrO multilayer selective absorption coatings in series, and designed the absorption layer with metal element concentration gradient. The absorptivity and emissivity of the coatings are 0.919 and 0.128, respectively. After heat treatment at 550 ℃ for 2 000 h under vacuum, the absorptivity and emissivity are 0.928 and 0.105, respectively. The excellent thermal stability of the coatings demonstrate the feasibility of this approach.

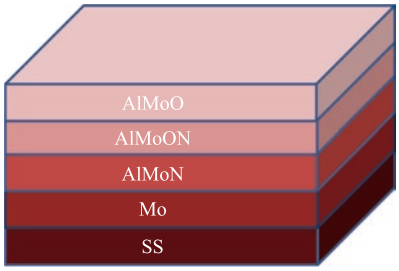


Fig.1 Structure diagram of AlMoON based solar selective absorption coating

Mo based coatings have been widely used in various fields[34]. The semiconductor nature of metal Mo provides a theoretical basis for its absorption of solar spectrum. According to the preparing methods of coatings and the similarity between Mo and Cr elements, Mo/AlMoN/AlMoON/AlMoO solar selective absorption coatings were deposited on stainless steel by magnetron sputtering in this research. In this multi-coatings, the Mo is IR reflector layer, AlMoN and AlMoON are absorber layer, and AlMoO is the anti-reflective layer. The structure of the coatings is shown in Fig.1. Most of the coatings prepared by magnetron sputtering are amorphous, which can avoid the irregular agglomeration of nanoparticles inside the coatings, and will beneficial to the improvement of the optical properties of the coatings. Due to the properties of Al and Mo, the thermal stability of the coatings is also further improved. The prepared coatings were heat treated under different conditions in atmospheric environment to evaluate the thermal stability.

## 2 Experimental

AlMoON based solar selective absorption coatings are deposited on stainless steel (25 mm×50 mm×0.8 mm) by magnetron sputtering. The structure of coatings are infrared reflection layer Mo, absorption layer AlMoN (HMVF), absorption layer AlMoON (LMVF) and antireflection layer AlMoO from bottom to top. Before depositing the coatings, the stainless steel substrate are ultrasonically cleaned by acetone, absolute ethanol and deionized water for 15 minutes. After cleaning, the substrate is dried and put into the sputtering equipment. The metal Mo target and metal Al target with purity of 99.99% are fixed on two DC power supplies respectively, and the vacuum chamber is vacuumized. When the vacuum reaches $10^{-4}$ Pa, the coatings begin to deposit. The different thicknesses of each single-layer structure of the coatings prepared under certain experimental parameters are optimized by orthogonal test. By comparing the optical properties of the coatings under different thicknesses of each single-layer structure, the thickness of each layer structure of the coatings with the best optical performance is selected as the final thickness parameter of the coatings. The final thickness of each layer structure is Mo infrared reflection layer 40 nm, AlMoN absorption layer 60 nm, AlMoON absorption layer 60 nm, AlMoO antireflection layer 60 nm. The experimental parameters are listed in Table 1.

The high temperature stability test of AlMoON based solar selective absorption coatings were carried

**Table 1 Preparation parameters of AlMoON based solar selective absorption coating**

| Layer | Power/W | Gas flow/sccm | | | Thickness/nm | Sputtering method |
|---|---|---|---|---|---|---|
| | | Ar | $N_2$ | $O_2$ | | |
| Mo | 60 | 150 | 0 | 0 | 40 | DC power |
| AlMoN | Mo:40, Al:60 | 120 | 30 | 0 | 60 | |
| AlMoON | Mo:40, Al:60 | 110 | 30 | 10 | 60 | |
| AlMoO | Mo:40, Al:60 | 140 | 0 | 10 | 60 | |

out in atmospheric environment. The muffle furnace is used to heat treat the coatings at a heating rate of 5 ℃/min. After a period of heat preservation process, it is cooled with the furnace. The experimental temperature parameters of high temperature heat treatment are 300, 400, and 500 ℃ respectively. Three quantities of 12, 24, and 36 h are set under each temperature parameter. The performance of the coatings after heat treatment under different conditions is evaluated, and finally a conclusion is drawn.

The deposited coatings and the coatings after heat treatment under different conditions were characterized. XRD and XPS were used to analyze the phase of the coatings before and after heat treatment. SEM and EDS were used to characterize the surface morphology and element proportion of the coatings before and after heat treatment. Al K$\alpha$ X-ray ($h\nu$=1 486.6 eV) is used in this XPS test, and the energy analysis range is 0-1 400 eV, and the coatings are etched by $Ar^+$. Regarding the correction of charge, Greczynski G and Hultman L[35-37] found that the binding energy of the C 1s peak of the amorphous carbon was related to the work function of the sample($\Phi_{SA}$), and the sum of $E_B^F$+$\Phi$SA was constant at 289.58±0.14 eV. The $\Phi_{SA}$ of CrAlN and TiAlN was range from 4.37 to 4.72 eV[38]. According to the preparing methods of coatings and proper references for materials[39-44], the $\Phi_{SA}$ of the deposited coatings in this study was selected to be 4.55±0.18 eV, therefore the carbon peak (C 1s) at 284.95 eV was used to correct the charge shift. Evolutions in microstructure of the coatings was observed by a focused ion beam-scan electron microscopy (FIB-SEM, FEI Scios 2 HiVac). FIB samples were observed by transmission electron microscopy (TEM). The point-line resolution of the coatings was 0.24 nm, which can be used to mapping the distribution of elements for different layers. UV-Vis-NIR spectrophotometer and Fourier infrared spectrophotometer were used to measure the reflectivity of the coatings at 0.3-25 μm[33]. According to the Kirchhoff's thermal radiation law[45,46], the absorptivity ($\alpha$) and emissivity ($\varepsilon$) of the coatings can be obtained by integrating the measured reflectivity. The calculation formulas are shown as follows,

$$\alpha(\theta)=\int_0^\infty \mathrm{d}\lambda\, A(\lambda)[1-r(\theta,\lambda)]/\int_0^\infty \mathrm{d}\lambda\, A(\lambda)$$

$$\varepsilon(\lambda,T)=\int_0^\infty \mathrm{d}\lambda\, E(\lambda,T)[1-r(\theta,\lambda)]/\int_0^\infty \mathrm{d}\lambda\, E(\lambda,T)$$

where, $\theta$ is the incident angle of light, $\lambda$ is the wavelength, $T$ is the test temperature, and $A(\lambda)$ and $E(\lambda,T)$. They are the energy density of solar radiation and blackbody radiation respectively.

The PC value is used to evaluate the coatings performance after heat treatment[22,23]. The PC value reflects the changes of optical properties of the coatings caused by the changes of absorptivity ($\alpha$) and emissivity ($\varepsilon$) caused by high temperature. The specific calculation formula shown is shown as follows,

$$PC=-\Delta\alpha+0.5\Delta\varepsilon$$

where, $\Delta\alpha=\alpha_{\text{High temperature}}-\alpha_{\text{As-deposition}}$, $\Delta\varepsilon=\varepsilon_{\text{High temperature}}-\varepsilon_{\text{As-deposition}}$. When the $PC$ value is greater than 0.05, the coating failure can be determined, and the corresponding high-temperature treatment time is the service life of the coatings.

# 3 Results and discussion

## 3.1 Optical properties

The reflectivity curve of the coating before and after heat treatment was measured, and the results are shown in Fig.2. It can be seen from it that the reflectance curve of the coating after atmospheric environment heat treatment at three different temperatures has a certain degree of red shift within the visible light range, and the minimum reflectivity appears in the range of 1-2 μm, which is greatly reduced compared with the deposited coating, but the reflectivity has increased to a certain extent in the range of 0.3-1 μm. It

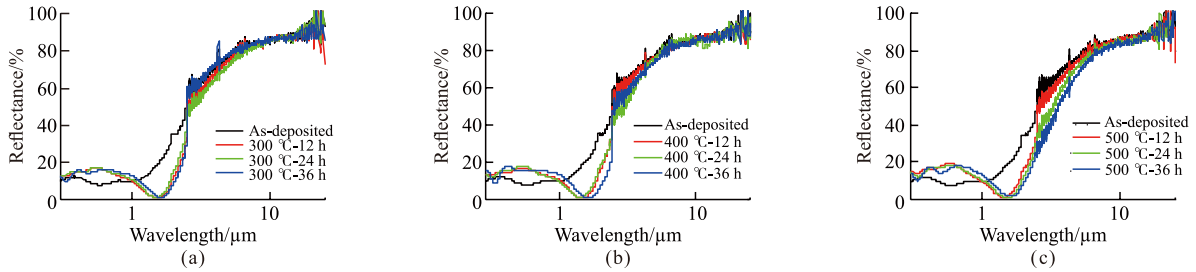


Fig.2 Reflection spectra of AlMoON based solar selective absorption coating after heat treatment at different temperatures in atmospheric environment: (a) 300 ℃; (b) 400 ℃; (c) 500 ℃

may be that high-temperature heat treatment increases the crystallization degree of compounds in the coating, resulting in the increase of the scattering degree of light transmitted into the coating, which improves the absorption of the coating in the visible light band to a certain extent. In the infrared band, after heat treatment at 300 and 400 ℃, the reflectivity curve of the coating does not change obviously, and the emissivity of the coating does not change obviously. After heat treatment at 500 ℃, the reflectivity curve of the coating decreases obviously, and the emissivity of the coating increases.

**Table 2 Optical properties of AlMoON based solar selective absorption coating**

| | | As-deposited | 12 h | 24 h | 36 h |
|---|---|---|---|---|---|
| 300 ℃ | $\alpha$ | 0.896 | 0.899 | 0.901 | 0.904 |
| | $\varepsilon$ | 0.09 | 0.102 | 0.100 | 0.08 |
| | $\alpha/\varepsilon$ | 9.96 | 8.81 | 9.01 | 11.3 |
| | PC | 0 | 0.003 | 0 | −0.013 |
| 400 ℃ | $\alpha$ | 0.896 | 0.907 | 0.897 | 0.892 |
| | $\varepsilon$ | 0.09 | 0.09 | 0.114 | 0.113 |
| | $\alpha/\varepsilon$ | 9.96 | 10.08 | 7.87 | 7.89 |
| | PC | 0 | −0.011 | 0.011 | 0.015 5 |
| 500 ℃ | $\alpha$ | 0.896 | 0.893 | 0.886 | 0.883 |
| | $\varepsilon$ | 0.09 | 0.116 | 0.124 | 0.131 |
| | $\alpha/\varepsilon$ | 9.96 | 7.70 | 7.15 | 6.74 |
| | PC | 0 | 0.016 | 0.027 | 0.033 5 |

The optical properties of the deposited coating and the coating after heat treatment under different conditions are listed in Table 2. It can be seen from the table that after heat treatment in 300 ℃ atmospheric environment, the absorption rate of the coating continues to rise, reaching 0.904 when treated for 36 h, while the emissivity fluctuates during the treatment, which is basically the same as that of the deposited coating, with the lowest being 0.08 when treated for 36 h. At this time, the quality factor also reaches the maximum value of 11.3. After heat treatment at 400 ℃ for 12 h, the absorption rate of the coating continues to rise, reaching 0.907 and the emissivity is 0.09, which is the same as that of the deposited coating. When the treatment time exceeds 12 h, the absorption rate of the coating shows a downward trend and the emissivity begins to rise. When the heat treatment temperature is 500 ℃, the optical properties of the coating continue to decline with the extension of the treatment time. When the treatment time is 36h, the absorptivity of the coating decreases to 0.883, the emissivity increases to 0.131, and the quality factor decreases to the lowest, which is 6.74. The PC value is introduced to evaluate the performance of the coatings[22,23], according to the definition of PC value, when the calculated PC value of the coating is greater than 0.05, the coating failure can be determined. It can be seen from the data in Table 2 that the coating has not failed after heat treatment under different experimental conditions, indicating that the coating has certain high-temperature stability[47].

## 3.2 Morphology analysis

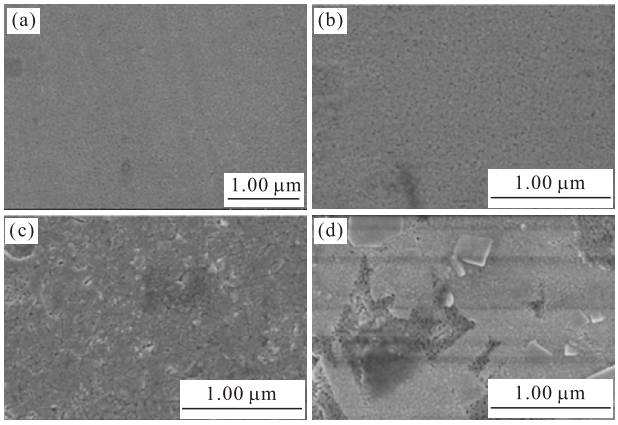


Fig.3 Surface morphology of AlMoON based solar selective absorption coating after heat treatment at different temperatures: (a) AS-deposited; (b) 300 ℃-36 h; (c) 400 ℃-36 h; (d) 500 ℃-36 h

Fig.3 shows the surface topography of the as-deposited coating and the coating after heat treatment under different conditions. Fig.3(a) shows the surface morphology of the deposited coating. From the figure, it can be seen that the coating surface is relatively flat, the particle size is relatively uniform, there is no obvious bulge and defects such as holes, cracks and irregular agglomeration of grains are observed. Fig.3(b) shows the surface morphology of the coating after heat treatment at 300 ℃-36 h. Compared with coating surface, the coating surface after heat treatment at 300 ℃-36 h is still relatively flat without obvious holes, cracks and other defects, but the roughness increases, which may be due to the increase of crystallization degree of surface materials after heat treatment and slight agglomeration, resulting in the increase of particle size and visual roughness of the coating surface. Fig.3(c) shows the surface morphology of the coating after heat treatment at 400 ℃-36 h. From the figure, it can be observed that the agglomeration of similar grains on the coating surface is more obvious, and slight cracks appear on the coating surface. These cracks can provide a channel for air to enter the interior of the coating and accelerate the oxidation of components in the coating, which may be the direct reason for the decline of the

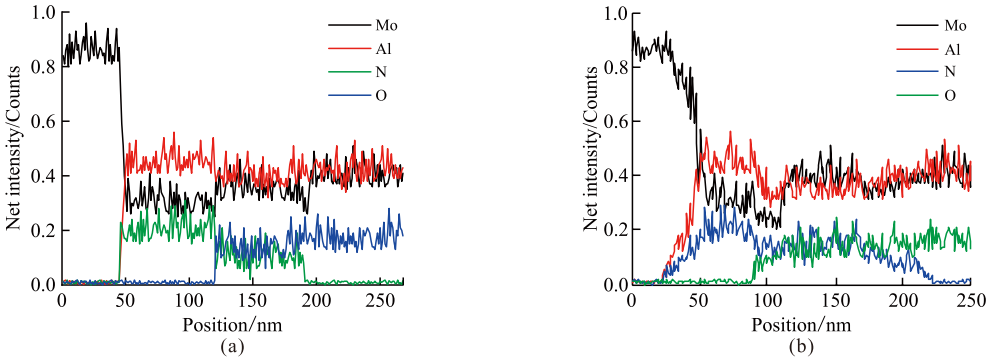


Fig.4 EDS line scan analysis of coating section: (a) As-deposited; (b) 500 ℃-36 h

optical properties of the coating after heat treatment at 400 ℃-36 h. Fig.3(d) shows the surface morphology of the coatings after heat treatment at 500 ℃-36 h. It is observed that there is a slight fracture on the coating surface at this time, and a small amount of blocks are attached to the coating surface. It is speculated that the fracture on the coating surface may be caused by high temperature, and the cracked coating continues to adhere to the coating surface. Because the coating surface is AlMoO antireflection layer, the slight fracture of the antireflection layer leads to a sharp increase in the emissivity of the coating, which leads to the decline of optical properties.

Fig.4 shows the cross-sectional EDS spectra of the as-deposited coating and the coating after heat treatment at 500 ℃-36 h. According to the comparison of Figs.4(a) and 4(b), when the thickness is 0-25 nm, the content of Mo in the coating after heat treatment is at the same level as that in the as-deposited coating. When the thickness exceeds 25 nm, the content of Mo begins to decrease, Al and N elements appear in the infrared reflection layer, and the existence of O element is also detected at the end of AlMoN absorption layer. According to the sputtering thickness of each layer, in the range of 190-250 nm the coating is antireflection layer AlMoO, but the presence of N element was detected in the range of 200-220 nm. It indicated that after heat treatment, the elements between adjacent layers had a certain diffusion, resulting in the content of different elements in each functional layer changed, resulting in a certain decline in the optical properties of the coatings.

### 3.3 Phase analysis

Fig.5 depicts the XRD patterns of the as-deposited and after heat treatment coatings. Using single crystal silicon as the coating substrate in XRD characterization, there are Si diffraction peaks in the XRD spectra of the coating. Except for the diffraction peak

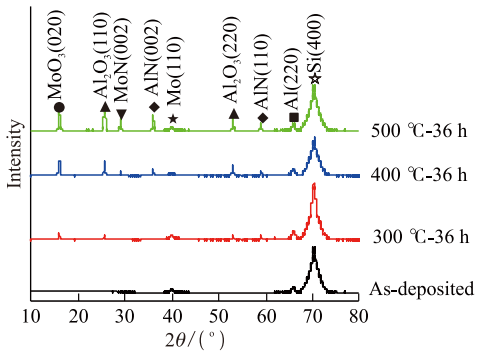


Fig.5 XRD patterns of multilayer coatings before and after heat treatment

of substrate Si, the deposited coating only appears weak diffraction at $2\theta$=40° and $2\theta$=66°, which are metal Mo and metal Al, respectively. After heat treatment at 300 ℃-36 h, in addition to the existing diffraction peaks of metal Mo and metal Al, there is a weak $Al_2O_3$ diffraction peak at $2\theta$=26° and $2\theta$=53° and AlN diffraction peak appears at $2\theta$=59°, $MoO_3$ diffraction peak appears at $2\theta$=16°, the intensity of diffraction peaks are weak. With the increase of heat treatment temperature, the weak diffraction peak of the coating after heat treatment at 300 ℃ increases gradually. In addition, MoN diffraction peak appears at $2\theta$=28° and AlN diffraction peak appears at $2\theta$=36°. With the increase of heat treatment temperature, the crystallinity of the substances present in the coating gradually increases, this may be the main reason for the above phenomenon. It may also be that with the increase of heat treatment temperature, defects appear on the coating surface, resulting in high-temperature air penetrating into the coating from the defects on the coating surface, accelerating the oxidation inside the coating and increasing the proportion of nitrogen oxide content inside the coating.

### 3.4 TEM analysis

Fig.6 shows TEM bright field images of the cross section of the multi-layer AlMoON based solar selective absorption coating. According to Fig.6(a), the four

layers of the coating can be distinguished. The interface of the coating layer is clear, and the stratification phenomenon in the Mo layer, AlMoN and AlMoO layer are obvious, while the changes of the AlMoON layer is not obvious. At the same time, the diffraction rings in selected diffraction spots are incomplete, and obvious single crystal spots can be seen in some locations, which indicates that the number of crystal phases in the coating increases. In order to quantitatively analyze the diffraction rings in the microregion, PASAD (profile analysis of the selected area electron diffraction pattern) script in Digital Micrograph software was used to analyze the diffraction ring. The selected area electron diffraction pattern was obtained from cross section of coating, suggesting the introduction of AlN, $MoO_3$ and $Al_2O_3$ phases. In the SAED pattern, as shown in Fig.6b, the diffraction rings were indexed characteristic (020) plane of $MoO_3$, (110) and (220) planes of $Al_2O_3$, (002) plane of AlN, and (002) plane of MoN, which was in agreement with XRD results.

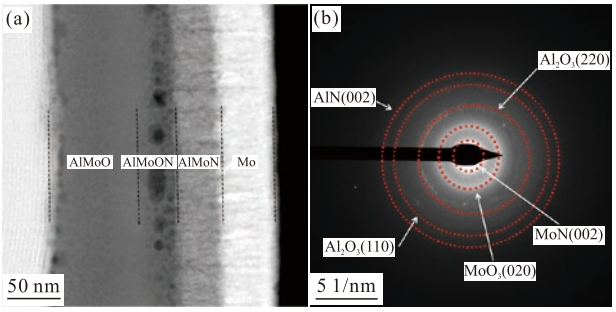


Fig.6 TEM images of AlMoON based solar selective absorption coating: (a) Bright-field TEM image; (b) Electron diffraction (SAED) image

Due to the difference in the composition of different layers, atomic diffusion or reaction may occur between the layers during heat treatment[48]. Fig.7 shows element distribution diagram of the cross section of the AlMoON based solar selective absorption coating for multiple absorption layers. After heat treatment, the composition distribution in the coating is relatively uniform, without element segregation and enrichment, but the interface area of the layer becomes wider. After heat treatment, O element diffuses from the higher content of AlMoON layer to the inner absorption layer, and N element also diffuses from the higher content of AlMoN layer to the AlMoON layer and Mo layer on both sides of the layers. However, Mo element in the infrared reflector does not diffuse to the absorption layer.

### 3.5 XPS analysis

The Mo 3d, Al 2p, N 1s and O 1s XPS spectra of coating after high temperature heat treatment at 500 ℃-36 h are shown in Figs.8-10. The standard binding energy of C 1s is 284.95 eV to calibrate the binding energy of other elements measured in this experiment[39-44]. According to the analysis and fitting, the binding energy of Mo 3d is 229.43, 232.18, 232.78, and 235.53 eV in AlMoN layer, the binding energy of Mo 3d is 229.63, 232.18, 232.93, and 235.53 eV in AlMoON layer, the binding energy of Mo 3d is 233.34 and 236.51 eV in AlMoO layer, and the Mo element mainly exists in the form of $Mo^{6+}$, $Mo^{4+}$, and $Mo^{3+}$ in the whole coating. The binding energy of Al 2p is 74.84 eV in AlMoN layer, the binding energies of Al 2p are 74.84 and 75.24 eV in the AlMoON layer, the binding

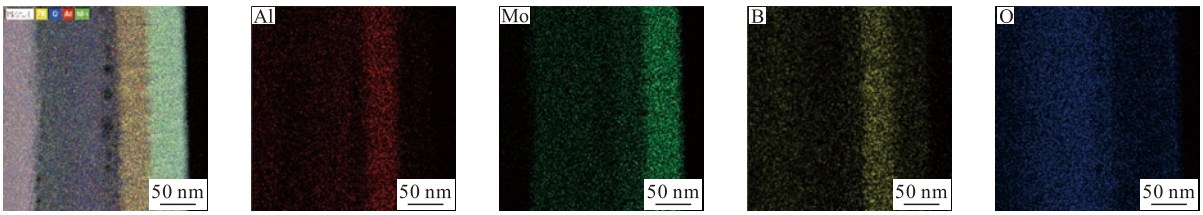


Fig.7 EDS maps of the distribution of Al, Mo, N and O in AlMoON based solar selective absorption coating

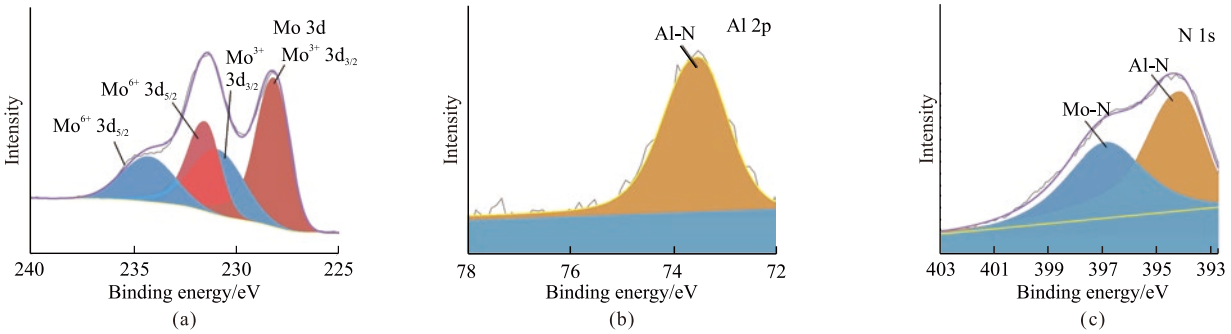


Fig.8 XPS spectra of elements on the surface of AlMoN layer after heat treatment at 500 ℃-36 h: (a)Mo 3d; (b)Al 2p; (c)N 1s

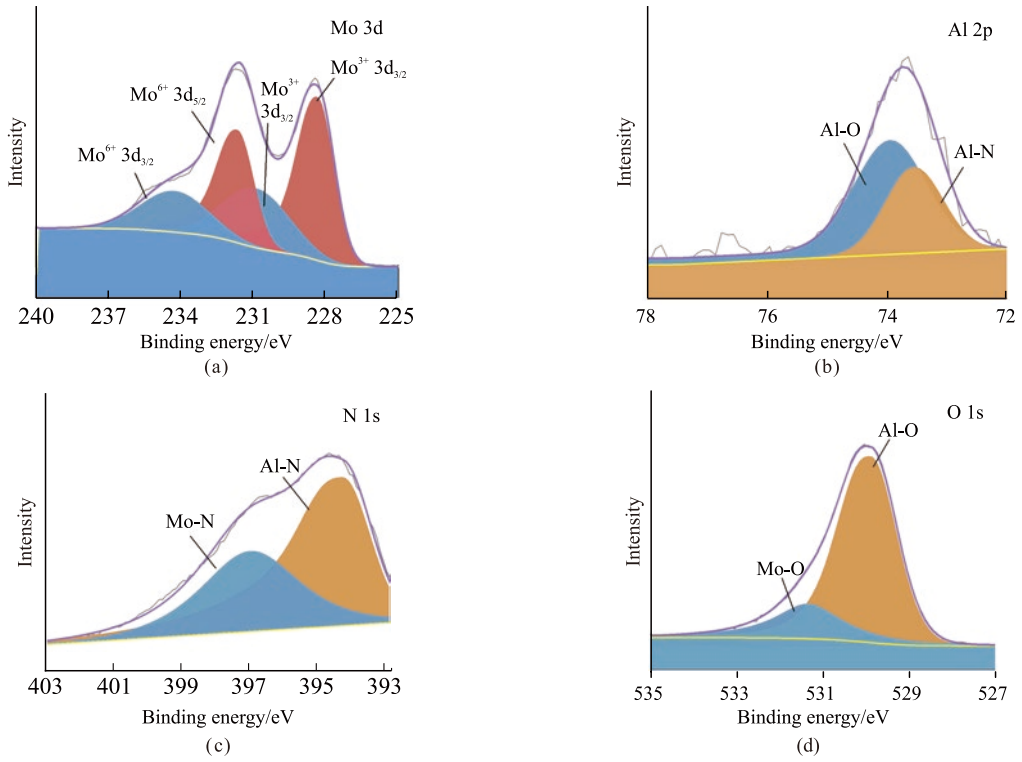


Fig.9 XPS spectra of elements on the surface of AlMoON layer after heat treatment at 500 ℃-36 h: (a) Mo 3d; (b) Al 2p; (c) N 1s; (d) O 1s

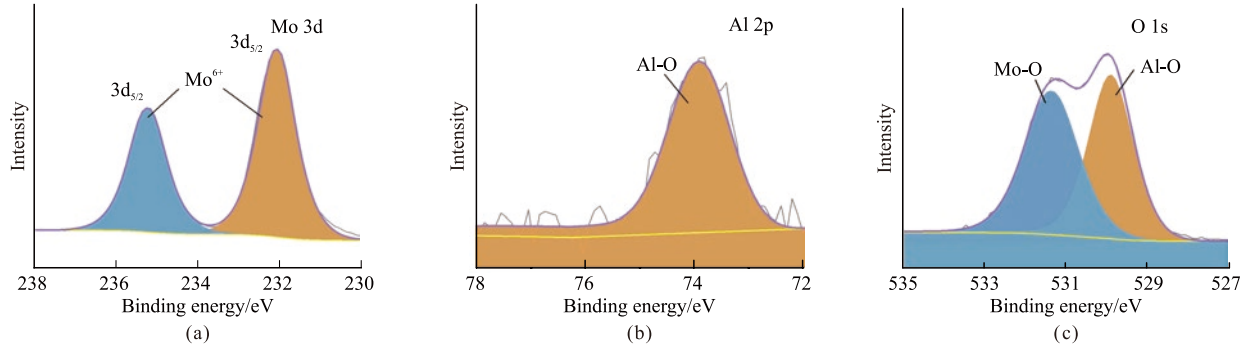


Fig.10 XPS spectra of elements on the surface of AlMoO layer after heat treatment at 500 ℃-36 h: (a) Mo 3d; (b) Al 2p; (c) O 1s

energy of Al 2p is 75.24 eV in the AlMoO layer. The binding energies of N 1s are mainly 395.44 and 398.43 eV, and that of O 1s are mainly 531.18 and 532.64 eV. They combine with metal Mo and metal Al to form Mo-N bond, Mo-O bond, Al-N bond, and Al-O bond. According to the inorganic elements (N and O) contained in each layer, the main components in AlMoN layer are MoN and AlN, the main components in AlMoON layer are $MoO_3$, MoN, $Al_2O_3$ and AlN, and the main components in AlMoO layer are $MoO_3$ and $Al_2O_3$.

Combined with the XRD and XPS spectra of the AlMoON based solar selective absorption coating after heat treatment in the atmospheric environment, in addition to the infrared reflective layer metal Mo, the coating after high temperature heat treatment mainly contains $MoO_3$, MoN, $Al_2O_3$, AlN, and other crystalline compounds. Compared with the XRD spectrum of the deposited AlMoON based solar selective absorption coating, the crystallinity of $Al_2O_3$, AlN and other compounds of $MoO_3$ and MoN increased, and obvious diffraction peaks of corresponding substances could be observed on the XRD spectrum. This is consistent with the above phenomenon[30], that is, with the increase of heat treatment temperature, the crystallinity of components in the coating gradually increases, and nanoparticles will diffuse into the coating with the crystalline coating components, resulting in the attenuation of optical properties of the coating. Due to the addition of metal aluminum and the related properties of aluminum elements in the coating components, the coating has a

certain thermal stability. After heat treatment under different conditions, the coating still did not fail.

# 4 Conclusions

AlMoON based solar selective absorption coatings were prepared by magnetron sputtering. The absorptivity and emissivity of the deposited AlMoON based solar selective absorption coatings were 0.896 and 0.09 respectively, and the quality factor was 9.96. After heat treatment under different conditions, the optical properties of the coatings did not change significantly, and the coatings have not failed. By element proportion analysis, a certain degree of element diffusion occurs in the coatings, resulting in the decline of the optical properties of the coatings. The absorptivity and emissivity are 0.883 and 0.131 respectively, the quality factor is 7.06 and the PC value is 0.0335. The coatings do not fail under this condition and has certain thermal stability. With the increase of heat treatment temperature and time, the crystallization degree of amorphous $MoO_3$, MoN, $Al_2O_3$, and AlN of the coatingS increase gradually. In summary, due to the thermal stability, the AlMoON based coatingS could be applied for solar photo-thermal conversion at high temperature, especially for concentrating solar power. In summary, due to the sound thermal stability, the AlMoON-based coatings could be applied for solar photo-thermal conversion at high temperature, especially for concentrating solar power.

### Conflict of interest

All authors declare that there are no competing interests.

### References


[1] Xue YF, Wang C, Sun Y, *et al*. Effects of the LMVF and HMVF Absorption Layer Thickness and Metal Volume Fraction on Optical Properties of the $MoSi_2$-$Al_2O_3$ Solar Selective Absorbing Coating[J]. *Vacuum*, 2014, 104: 116-121

[2] Antonaia A, Castaldo A, Addonizio ML, *et al*. Stability of W-$Al_2O_3$ Cermet Based Solar Coating for Receiver Tube Operating at High Temperature[J]. S*olar Energy Materials and Solar Cells*, 2010, 94(10): 1 604-1 611

[3] Zhao K, Jin HG, Gai ZR, *et al*. A Thermal Efficiency-enhancing Strategy of Parabolic Trough Collector Systems by Cascadingly Applying Multiple Solar Selective-absorbing Coatings[J]. *Applied Energy*, 2022, 309: 118 508

[4] Cao F, McEnaney K, Chen G, *et al*. A Review of Cermet-based Spectrally Selective Solar Absorbers[J]. *Energy & Environmental Science*, 2014, 7(5): 1 615-1 627

[5] Cheng CL, Liu CC, Dai MZ. Physical and Photovoltaic Characteristics ofCopper Oxide Thin Films as Hole-selective Layers for Sscreen-printed Mono-crystalline Silicon Solar Cell Applications[J]. *Vacuum*, 2022, 197: 110 805

[6] Farhadizadeh A, Kozák T. The Importance of Discharge Voltage in DC Magnetron Sputtering for Energy of Sputtered and Backscattered Atoms on the Substrate: Monte-Carlo Simulations[J]. *Vacuum*, 2022, 196: 110 716

[7] Selvakumar N, Barshilia HC. Review of Physical Vapor Deposited (PVD) Spectrally Selective Coatings for Mid- and high-temperature Solar Thermal Applications[J]. *Solar Energy Materials & Solar Cells*, 2012, 98(5): 1-23

[8] Xue YF, Wang C, Sun Y, *et al*. Preparation and Spectral Properties of Solar Selective Absorbing $MoSi_2$-$Al_2O_3$ Coating [J]. *Applications and materials science*, 2014, 211: 1 519-1 524

[9] Zheng LQ, Gao F, Zhao S, *et al*. Optical Design and Co-sputtering Preparation of High Performance Mo-$SiO_2$ Cermet Solar Selective Absorbing Coating[J]. *Applied Surface Science*, 2013, 280: 240-246

[10] Setién-Fernández I, Echániz T, González-Fernández L, *et al*. First Spectral Emissivity Study of a Solar Selective Coating in the 150-600℃ Temperature Range[J]. *Solar Energy Materials and Solar Cells*, 2013, 117: 390-395

[11] Céspedes E, Wirz M, Sánchez-García JA, *et al*. Novel Mo-$Si_3N_4$ Based Selective Coating for High Temperature Concentrating Solar Power Applications[J]. *Solar Energy Materials and Solar Cells*, 2014, 122: 217-225

[12] Xu A, Chen QZ, Huang ZJ, *et al*. Effect of Al Layer on Oxidation Behavior of NbCrAl Coating[J]. *Journal of Wuhan University of Technology-Mater. Sci. Ed.*, 2019, 34 (2): 391-396

[13] Barshilia HC, Selvakumar N, Rajam KS, *et al*. Deposition and Characterization of TiAlN/TiAlON/$Si_3N_4$ Tandem Absorbers Prepared Using Reactive Direct Current Magnetron Sputtering[J]. *Thin Solid Films*, 2008, 516(18): 6 071-6 078

[14] Yin Y, Hang L, Zhang S, *et al*. Thermal Oxidation Properties of Titanium Nitride and Titanium-aluminum Nitride Materials - A Perspective for High Temperature Air-stable Solar Selective Absorber Applications[J]. *Thin Solid Films*, 2007, 515(5): 2 829-2 832

[15] Wu YW, Zheng WF, Lin LM, *et al*. Colored Solar Selective Absorbing Coatings with Metal Ti and Dielectric AlN Multilayer Structure[J]. *Solar Energy Materials and Solar Cells*, 2013, 115: 145-150

[16] Du M, Liu XP, Hao L, *et al*. Microstructure and Thermal Stability of Al/$Ti_{0.5}Al_{0.5}N$/$Ti_{0.25}Al_{0.75}N$/AlN Solar Selective Coating[J]. *Solar Energy Materials and Solar Cells*, 2013, 111: 49-56

[17] Liu HD, Wan Q, Lin BZ, *et al*. The Spectral Properties and Thermal Atability of CrAlO-based Solar Selective Absorbing Nanocomposite Coating[J]. *Solar Energy Materials and Solar Cells*, 2014, 122: 226-232

[18] Barshilia HC, Kumar P, Rajam KS, *et al*. Structure and Optical Properties of Ag-$Al_2O_3$ Nanocermet Solar Selective Coatings Prepared Using Unbalanced Magnetron Sputtering[J]. *Solar Energy Materials & Solar Cells*, 2011, 95(7): 1 707-1 715

[19] Nunes C, Teixeira V, Prates ML, *et al*. Graded Selective Coatings Based on Chromium and Titanium Oxynitride[J]. *Thin Solid Films*, 2003, 442(1): 173-178

[20] Li QY, Gong DQ, Cheng XD. Thickness Dependence of Structural and Optical Properties of Chromium Thin Films as an Infrared Reflector for Solar-thermal Conversion Applications[J]. *Journal of Wuhan University of Technology-Mater. Sci. Ed.,* 2019, 38(6): 1 239-1 247

[21] Gaouyat L, Mirabella F, Deparis O. Critical Tuning of Magnetron Sputtering Process Parameters for Optimized Solar Selective Absorption of $NiCrO_x$ Cermet Coatings on Aluminium Substrate[J]. *Applied Surface Science*, 2013, 271: 113-117

[22] Gaouyat L, He Z, Colomer JF, *et al*. Revealing the Innermost Nanostructure of Sputtered $NiCrO_x$ Solar Absorber Cermets[J]. *Solar Energy Materials and Solar Cells*, 2014, 122: 303-308

[23] Wang XB, Li KW, Cheng XD. Resistant Transition-metal-nitrides Based Coatings for Solar Energy Conversion[J]. *Journal of the European Ceramic Society*, 2021, 41(7): 4 076-4 085

[24] Schüler A, Thommen V, Reimann P, *et al*. Structural and Optical Properties of Titanium Aluminum Nitride Films ($Ti_{(1-x)}Al_xN$)[J]. *Journal of Vacuum Science & Technology, A. Vacuum, Surfaces, and Films*, 2001,19(3): 922-929

[25] Gong DQ, Cheng XD, Ye WP, *et al*. The Effect of Annealing Under Non-Vacuum on the Optical Properties of TiAlN Non-Vacuum Solar Selective Absorbing Coating prepared by Cathodic Arc Evaporation[J]. *Journal of Wuhan University of Technology-Mater. Sci. Ed.*, 2013, 28(2): 256-260

[26] Valleti K, Murali Krishna D, and Joshi SV. Functional Multi-layer Nitride Coatings for High Temperature Solar Selective Applications[J]. *Solar Energy Materials and Solar Cells*, 2014, 121: 14-21

[27] Gong H, Shao W, Ma XT, *et al*. Absorption Properties of a Multilayer Composite Nanoparticle for Solar Thermal Utilization[J]. *Optics and Laser Technology*, 2022, 150: 107 914

[28] Danlée Y, Mederos-Henry F, *et al*. *Ranking Broadband Microwave Absorption Performance of Multilayered Polymer Nanocomposites Containing Carbon and Metallic Nanofillers*[M]. Prime Archives in Material Science: 3rd Edition, 2021

[29] Zhang Q, Mills DR. New Cermet Film Structures with Much Improved Selectivity for Solar Thermal Applications[J]. *Applied Physics Letters*, 1992, 60: 545-547

[30] Liu HD, Yang B, Mao MR, *et al*. Enhanced Thermal Stability of Solar Selective Absorber Based on Nano-multilayered TiAlON Films Deposited by Cathodic Arc Evaporation[J]. *Applied Surface Science*, 2020, 501: 144 025

[31] Du M, Hao L, Mi J, *et al*. Optimization Design of $Ti_{0.5}Al_{0.5}N$/$Ti_{0.25}Al_{0.75}N$/AlN Coating Used for Solar Selective Applications[J]. *Solar Energy Materials and Solar Cells*, 2011, 95(4): 1 193-1 196

[32] Jyothi J, Chaliyawala Ha, Srinivas G, *et al*. Design and Fabrication of Spectrally Selective TiAlC/TiAlCN/TiAlSiCN/TiAlSiCO/TiAlSiO Tandem Absorber for High-temperature Solar Thermal Power Applications[J]. *Solar Energy Materials and Solar Cells*, 2015, 140: 209-216

[33] Wang XB, Yuan XP, Gong DQ, *et al*. Optical Properties and Thermal Stability of AlCrON-Based Multilayer Solar Selective Absorbing Coating for High Temperature Applications[J]. *Journal of Materials Research and Technology*, 2021, 15: 6 162-6 174

[34] Min J, Gu L, Chen YF, *et al*. Damping Performance of Mo-based Coatings Prepared by Supersonic Arc Spraying[J]. *Surface Engineering*, 2021, 37(11): 1 388-1 395

[35] Greczynski G, Hultman L. X-ray Photoelectron Spectroscopy: Towards Reliable Binding Energy Referencing[J]. *Progress in Materials Science*, 2020, 107: 100 591

[36] Greczynski G, Hultman L. C 1s peak of Adventitious Carbon Aligns to the Vacuum Level: Dire Consequences for Material's Bonding Assignment by Photoelectron Sectroscopy[J]. *Chem. Phys. Chem.*, 2017, 18(12): 1 507-1 512

[37] Greczynski G, Hultman L. The Same Chemical State of Carbon Gives Rise to Two Peaks in X-ray Photoelectron Spectroscopy[J]. *Scientific Reports*, 2021, 11(1): 1-5

[38] Greczynski G, Hultman L. Reliable Determination of Chemical State in x-ray Photoelectron Spectroscopy Based on Sample-work-function Referencing to Adventitious Carbon: Resolving the Myth of Apparent Constant Binding Energy of the C 1s Peak[J]. *Applied Surface Science*, 2018, 451: 99-103

[39] Huang B, Liu LT, Du HM, *et al*. Effect of Nitrogen Flow Rate on the Microstructure, Mechanical and Tribological Properties of CrAlTiN Coatings Prepared by Arc Ion Plating[J]. *Vacuum*, 204: 111 336

[40] Liu Y, Ding JC, Zhang BR, Chen JJ, *et al*. Effect of Duty Cycle on Microstructure and Mechanical Properties of AlCrN Coatings Deposited by HiPIMS[J]. *Vacuum*, 2022, 205: 111 409

[41] Greczynski G, Hultman L. Compromising Science by Ignorant Instrument Calibration-Need to Revisit Half a Century of Published XPS Data[J]. *Angew. Chem. Int. Ed.*, 2020, 59: 5 002-5 006

[42] Selvakumar N, Rajaguru K, Gouda GM, *et al*. AlMoN Based Spectrally Selective Coating with Improved Thermal Stability for High Temperature Solar Thermal Applications[J]. *Solar Energy*, 2015(119): 114-121

[43] Selvakumar N, Santhoshkumar S, Basu S, *et al*. Spectrally Selective CrMoN/CrON Tandem Absorber for Mid-temperature Solar Thermal Applications[J]. *Solar Energy Materials & Solar Cells*, 2013(109): 97-103

[44] Blaz L, Wloch G, Lobry P, *et al*. Structural Aspect of Chemical Reaction Between Components of Mechanically Alloyed Al-$MoO_2$ and Al-$MoO_3$ Composites[J]. *Journal of Alloys and Compounds*, 2017 (695): 1 096-1 103

[45] Mukhopadhyay S, Sahimi M. Calculation of the Effective Permeabilities of Field-scale Porous Media [J]. *Chemical Engineering Science*, 2000, 55(20): 4 495-4 513

[46] Kennedy CE, Price H. Progress in Development of High-temperature Solar-selective Coating [C]. In: *American Society of Mechanical Engineers. Internation.al Solar Energy Conference, Solar Engineering 2005-Proceedings of the 2005 International Solar Energy Conference,* New York: American Society of Mechanical Engineers, 2005

[47] Zhang CY, Cao HW, Dong H, *et al*. Influence of a TiAlN Coating on the Mechanical Properties of a Heat Resistant Steel at Room Temperature and 650℃[J]. *Journal of Wuhan University of Technology-Mater. Sci. Ed.*, 2013, 28(5): 1 029-1 033

[48] Zhu TK, Wang DG, Luo X. Effect of C/Mo Duplex-coating on Thermal Residual Stresses in $SiC_f$/$Ti_2AlNb$ Composites[J]. *Journal of Wuhan University of Technology-Mater. Sci. Ed.,* 2021, 36(4): 526-532